

Supplementary Materials for

Tunable structure and dynamics of active liquid crystals

Nitin Kumar, Rui Zhang, Juan J. de Pablo*, Margaret L. Gardel*

*Corresponding author. Email: depablo@uchicago.edu (J.J.d.P.); gardel@uchicago.edu (M.L.G.)

Published 12 October 2018, *Sci. Adv.* **4**, eaat7779 (2018)

DOI: 10.1126/sciadv.aat7779

The PDF file includes:

Fig. S1. Myosin motors cluster over time.
Fig. S2. Temporal behavior of root mean square velocity.
Fig. S3. Myosin motors do not localize to defect cores.
Fig. S4. Time averaging of defect spacing.
Fig. S5. Effect of flow alignment on the change of defect morphology.
Fig. S6. Director field associated with different defect orientations.
Supplementary Text
Legends for movies S1 to S10

Other Supplementary Material for this manuscript includes the following:

(available at advances.sciencemag.org/cgi/content/full/4/10/eaat7779/DC1)

Movie S1 (.avi format). Crowding of actin filaments (mean length, $l = 1 \mu\text{m}$) on an oil-water interface forming a 2D nematic LC.
Movie S2 (.avi format). A dense film of actin filaments (red, $l = 1 \mu\text{m}$) and myosin II (green) form an active nematic.
Movie S3 (.avi format). Generation of topological defect pairs in actomyosin-based active nematic ($l = 1 \mu\text{m}$).
Movie S4 (.avi format). Persistent motion of a $+1/2$ defect (solid symbol) along its orientation in our actomyosin-based active nematics ($l = 1 \mu\text{m}$); $-1/2$ (open symbol) defect remains immobile.
Movie S5 (.avi format). Fluorescence images of actin (left) and myosin (right) in actin nematic ($l = 2 \mu\text{m}$).
Movie S6 (.avi format). Time-lapse imaging of fluorescent actin in a passive nematic LC ($l = 1 \mu\text{m}$, $c = 0 \mu\text{m}^{-2}$) showing annihilation of defect pairs.
Movie S7 (.avi format). Time-lapse imaging of fluorescent actin in an active nematic LC ($l = 1 \mu\text{m}$, $c = 0.01 \mu\text{m}^{-2}$) showing defect repulsion.

Movie S8 (.avi format). Time-lapse imaging of fluorescent actin in an active nematic LC ($l = 1 \mu\text{m}$, $c = 0.0015 \mu\text{m}^{-2}$) showing defect stalling, where the defect pair separation (indicated by open symbols) does not change significantly over the course of 3 min.

Movie S9 (.avi format). Simulation movie of defect dynamics in a quasi-2D active nematic LC.

Movie S10 (.avi format). Time-lapse imaging of \pm defect pair dynamics in active nematic LC ($l = 1 \mu\text{m}$, $c = 0.0015 \mu\text{m}^{-2}$) showing that defect orientations change from roughly antiparallel at large separation to parallel when close, consistent with the structural analysis of defects in simulations.

SUPPLEMENTARY FIGURES

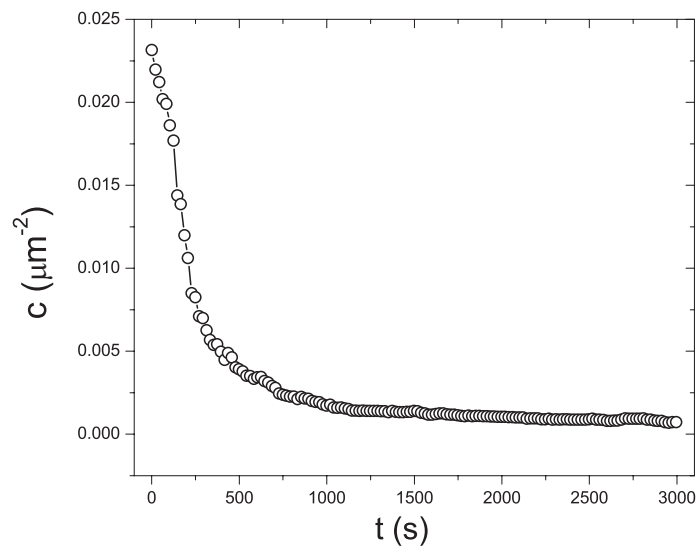


Fig. S1. **Myosin motors cluster over time.** The number density of motors c decays as a function of time.

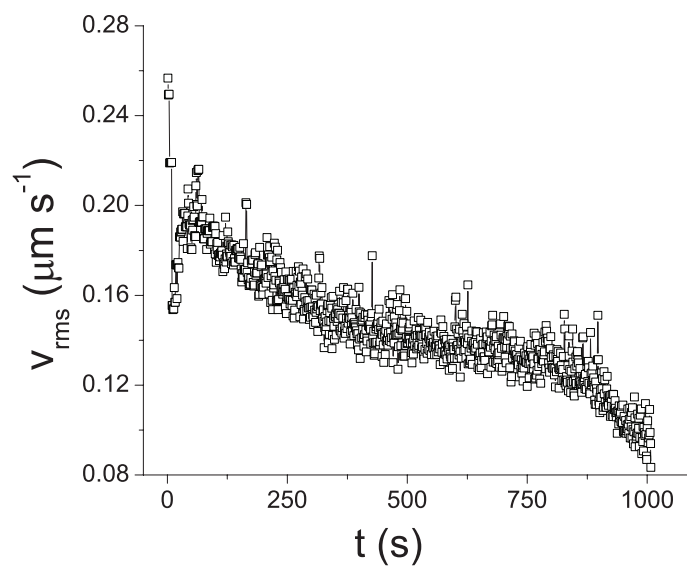


Fig. S2. **Temporal behavior of root mean square velocity.** Root mean square velocity ($v_{rms} = \sqrt{\langle v^2 \rangle}$, where v is the magnitude of local PIV velocity field) of the active nematic as a function of time. The figure shows that the kinematic energy is declining as motor proteins aggregate.

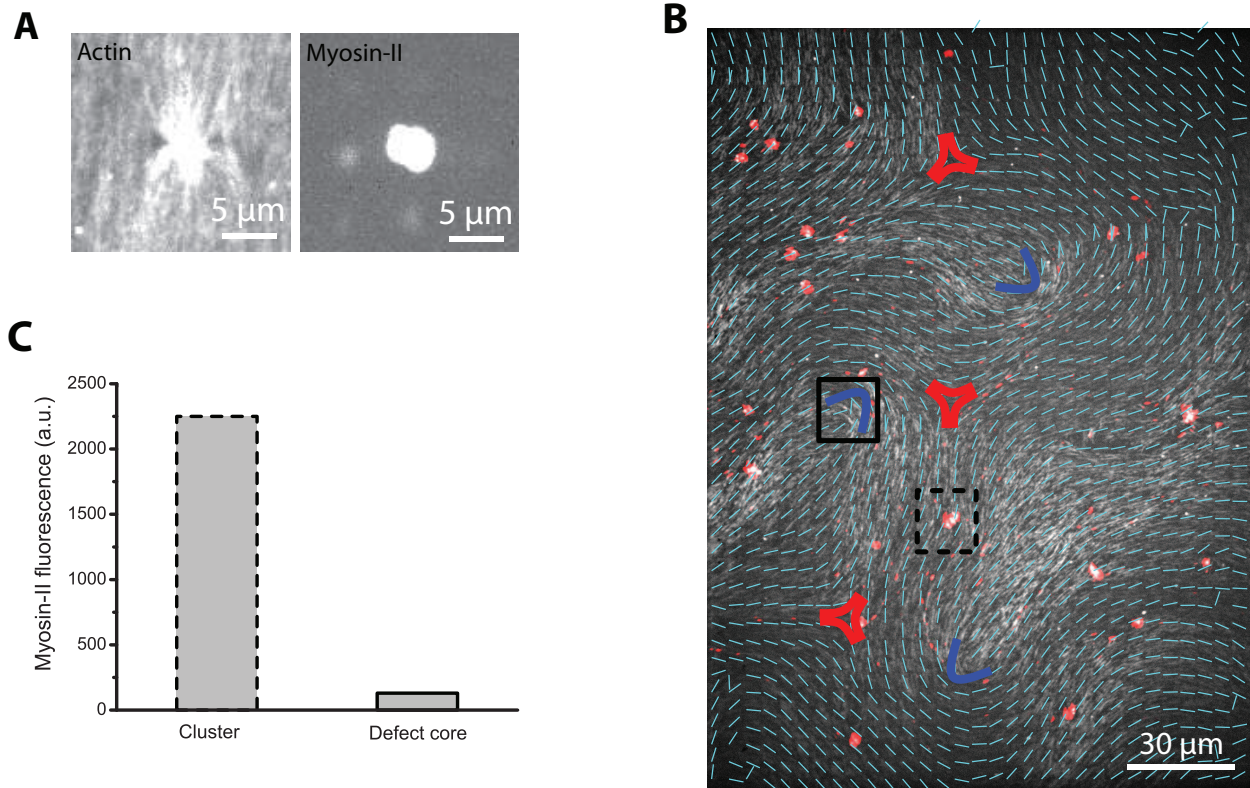


Fig. S3. Myosin motors do not localize to defect cores. (A) Actin and myosin-II channels corresponding to a typical cluster. (B) Experimental image with nematic director field overlaid, showing that the myosin clusters (in red) never occupy the defect cores. The $+1/2$ and $-1/2$ defects are indicated by blue and green symbols, respectively. (C) Average of the maximum value of myosin-II fluorescent signal at the location of a cluster (black dashed box) and close to the defect (black box).

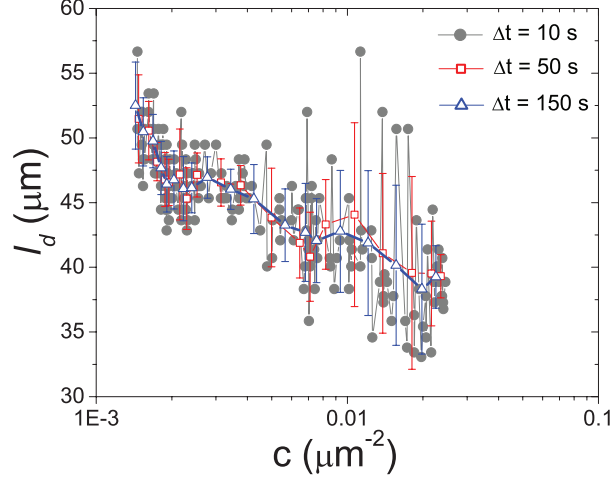


Fig. S4. **Time averaging of defect spacing.** Mean defect spacing, l_d , as a function of concentration for three values of time averaging time-interval. The data presented in main Fig. 1C correspond to a time-averaged data over a time window, $\Delta t = 150$ s, which corresponds to the minimum standard deviation without losing the general trend. The value $\Delta t = 150$ s is also used for ξ_v and ξ_θ . These timescales are much longer than the average relaxation time (~ 1 s) of the LC.

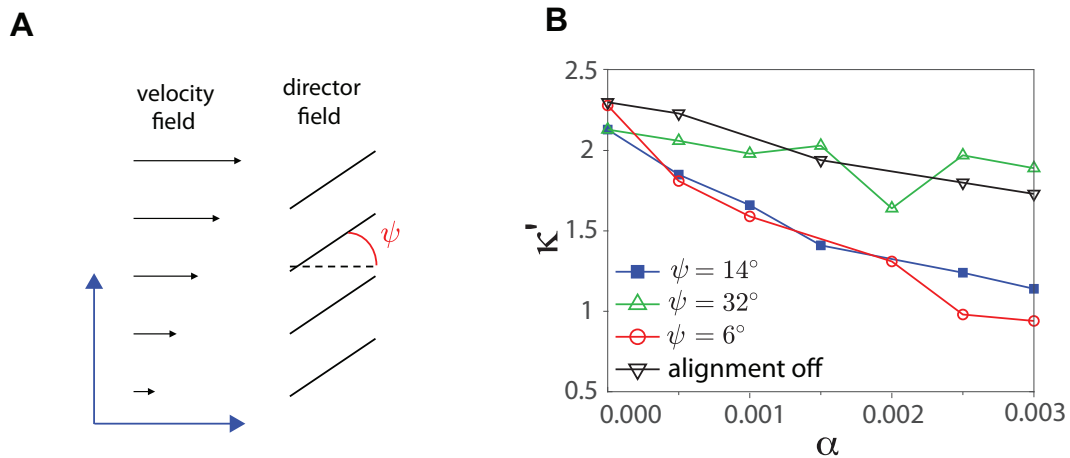


Fig. S5. **Effect of flow alignment on the change of defect morphology.** (A) Illustration of Leslie angle ψ of liquid crystal subject to strong shear flow. (B) Apparent elasticity κ' as function of activity α at different Leslie angles and when flow alignment is turned on or off.

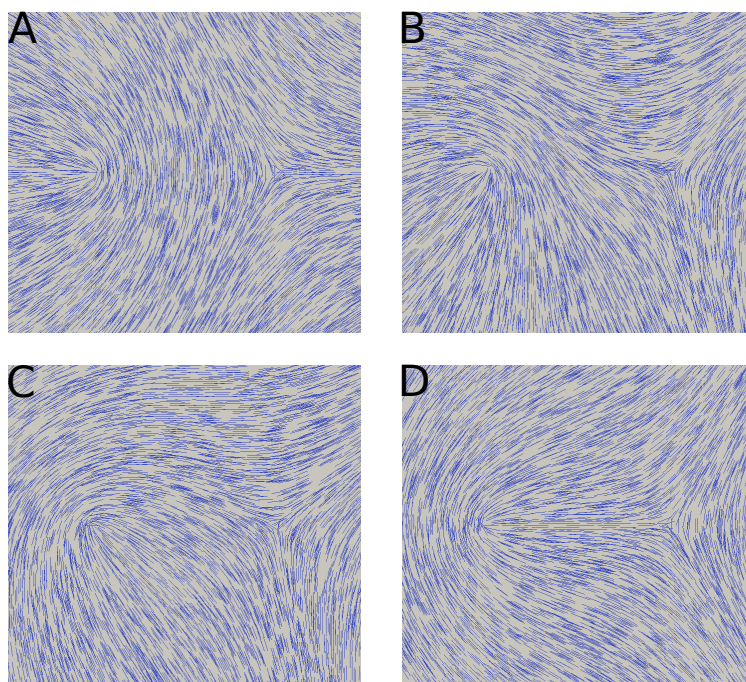


Fig. S6. **Director field associated with different defect orientations.** (A) $\Theta = 0^\circ$; (B) $\Theta = 45^\circ$; (C) $\Theta = 135^\circ$; (D) $\Theta = 180^\circ$.

SUPPLEMENTARY TEXT

In fig. S5, we show results from simulations that provide insights into how hydrodynamic effects influence defect morphology. The angle between the director and the flow direction for a strong shear flow is the Leslie angle ψ [33], as illustrated in fig. S5A. Such an angle and ξ are related according to the following equation[46]

$$\xi \cos(2\psi) = 3q_0/(2 + q_0)$$

In simulations, we tuned ξ to control the Leslie angle ψ . As shown in Fig. 2D, the hydrodynamic flow associated with the active motion of the $+1/2$ defect gives rise to a strong shear flow. The directors respond to such a flow by aligning with it. We find that the lower ψ , the smaller κ' , consistent with the flow alignment picture. To further examine the contribution of such hydrodynamic effects, we also perform a separate simulation in which the flow-alignment term $\mathbf{S}(\mathbf{W}, \mathbf{Q})$ in Eq. 7 is turned off. As shown in fig. S5B, the $\kappa' - \alpha$ curve becomes much flatter. This implies that flow-alignment effects are an important but not the only contributor to the change of defect morphology. The other contributor is the increase of activity-promoted bending in active systems.

We have performed simulations of defect dynamics with different orientations of the $+1/2$ defect, as illustrated in fig. S6. The orientation of the $-1/2$ defect in the initial state is chosen such that the overall elastic energy of the defect-pair system is a minimum. The dynamics of defect pair is determined by whether the defects annihilate in later stages of the simulation.

SUPPLEMENTARY MOVIE LEGENDS

Movie S1. Crowding of actin filaments (mean length, $l = 1 \mu\text{m}$) on an oil-water interface forming a 2D nematic LC.

Movie S2. A dense film of actin filaments (red, $l = 1 \mu\text{m}$) and myosin II (green) form an active nematic.

Movie S3. Generation of topological defect pairs in actomyosin-based active nematic ($l = 1 \mu\text{m}$). After motor proteins are added ($t = 0$), a pair of $\pm 1/2$ defects emerges. Left channel: F-actin; right channel: myosin-II.

Movie S4. Persistent motion of a $+1/2$ defect (solid symbol) along its orientation in our actomyosin-based active nematics ($l=1 \mu\text{m}$); $-1/2$ (open symbol) defect remains immobile.

Movie S5. Fluorescence images of actin (left) and myosin (right) in actin nematic ($l = 2 \mu\text{m}$). Upon the addition of motors at $t = 00:00$, the $+1/2$ defect morphology changes from V to U.

Movie S6. Time-lapse imaging of fluorescent actin in a passive nematic LC ($l = 1 \mu\text{m}$, $c = 0 \mu\text{m}^{-2}$) showing annihilation of defect pairs.

Movie S7. Time-lapse imaging of fluorescent actin in a active nematic LC ($l = 1 \mu\text{m}$, $c = 0.01 \mu\text{m}^{-2}$) showing defect repulsion.

Movie S8. Time-lapse imaging of fluorescent actin in a active nematic LC ($l = 1 \mu\text{m}$, $c = 0.0015 \mu\text{m}^{-2}$) showing defect stalling, where the defect pair separation (indicated by open symbols) does not change significantly over the course of 3 min.

Movie S9. Simulation movie of defect dynamics in a quasi-2D active nematic LC. Red lines indicate the orientations of $+1/2$ defects; Blue lines indicate the triad structures of $-1/2$ defects; Short black lines represent the local director field.

Movie S10. Time-lapse imaging of \pm defect pair dynamics in active nematic LC ($l = 1 \mu\text{m}$, $c = 0.0015 \mu\text{m}^{-2}$) showing that defect orientations change from roughly antiparallel at large separation to parallel when close, consistent with the structural analysis of defects in simulations.